Rock Mechanics and Rock Engineering
https://doi.org/10.1007/s00603-019-01841-5

TECHNICAL NOTE

Influence of the Effective Vertical Stresses on Hydraulic Fracture Initiation Pressures in Shale and Engineered Geothermal Systems Explorations

Gayani Gunarathna[1] · **Bruno Gonçalves da Silva**[1]

Received: 24 May 2018 / Accepted: 30 April 2019

Keywords Hydraulic fracturing · Shale stimulation · Enhanced geothermal systems · Breakdown pressure

1 Introduction

In recent years, hydrocarbon extraction is relying progressively more on hydraulic fracturing stimulation of shale reservoirs to increase their permeability and, therefore, their productivity. Engineered geothermal systems (EGS) have also been using hydraulic fracturing to create and mobilize fractures in the hot rock through which water is circulated to subsequently recover its heat at the surface. Hydraulic fracturing consists of the injection of fluid into rock at an adequate pressure to create new fractures as well as to open, or mobilize, existing ones. These newly formed and mobilized fractures can serve as highly permeable pathways to enhance the reservoir productivity (Frash 2007). Taking advantage of the hydraulic fracturing technology, shale oil and gas production have grown considerably in the past decade (McClure 2012) and EGS have been increasingly used in pilot developments (Tester 2006). While hydraulic fracturing has been extensively used in field applications, the fracturing processes involved in this method are still not well understood. One of the variables that needs to be better studied is the breakdown pressure ($P_{\text{breakdown}}$), particularly its variation with depth, i.e., with overburden stresses. In fact, it is important to observe trends that may help one understand the effect of the in situ vertical stresses on the breakdown pressure to better predict and design hydraulic fracturing operations.

In this study, several shale oil and/or gas and EGS hydraulic fracturing projects are analyzed. Specifically, the influence of the effective vertical stress (σ'_{v}) on the breakdown pressures is investigated and compared to theoretical models. This technical note initially discusses existing models used to predict the fracture initiation pressures and the minimum pressures to "hold open and extend fractures" in Sect. 2; in Sect. 3, various shale oil and/or gas and EGS projects are reviewed. The breakdown pressures measured in the different projects are then analyzed and related to their respective in situ vertical effective stress σ'_{v} to evaluate possible trends, in Sect. 4. Finally, a discussion of the findings of the study is presented in Sect. 5, including a comparison between the field and theoretical values. In the context of this paper, the term breakdown pressure ($P_{\text{breakdown}}$) indicates the maximum fluid pressure reached at the bottom of the wellbore, as will be further explained in Sect. 2.1.

2 Background

2.1 Relevant Terminology

The variation of wellbore pressure with time for a general hydraulic fracturing test is shown schematically in Fig. 1 (Feng and Gray 2017). Fracture initiation pressure (FIP) occurs when a deviation in linearity is observed in pressure–time plot, which indicates a possible fracture initiation. The pressure continues to increase as the fracture stably propagates until it reaches the formation breakdown pressure (FBP). At this point, the pressure drops to the fracture propagation pressure (FPP) as there is an unstable fracture propagation characterized by a rapid increase in fracture volume. The breakdown pressure is typically reported in field operations, since it is the maximum pressure reached during a hydraulic fracturing procedure.

✉ Gayani Gunarathna
ksg24@njit.edu

[1] New Jersey Institute of Technology, Newark, NJ, USA

Published online: 18 May 2019

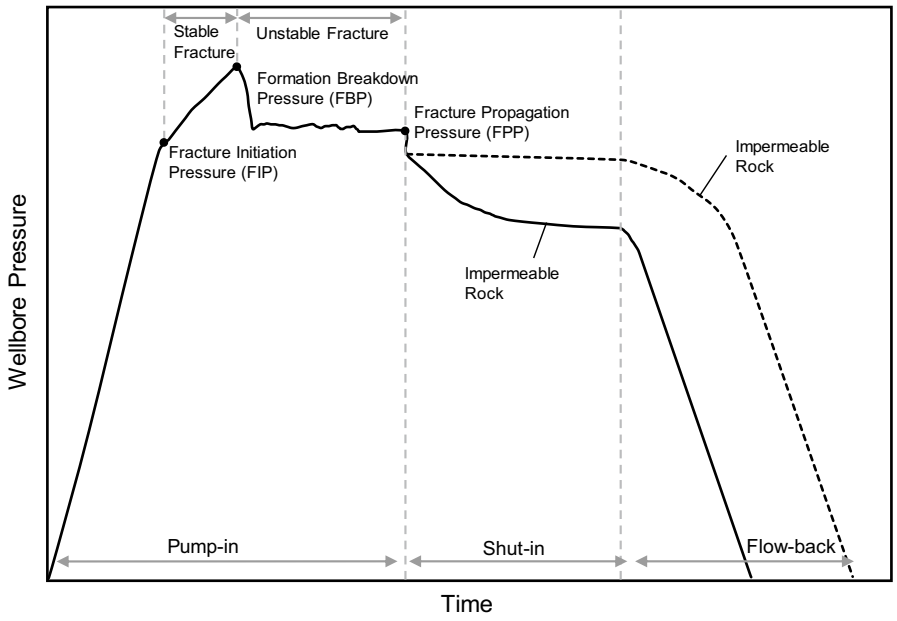

Fig. 1 Pressure–time response of field hydraulic fracturing test (after Feng and Gray 2017)

2.2 Theoretical Models for Hydraulic Fracture Initiation

Fracture initiation and re-opening pressures are crucial in the process of estimating the equipment requirements for hydraulic fracturing operations. It is known that rock fractures, in general, and hydraulic fractures, in particular, may occur along planes normal to the least principal stress direction (Scott et al. 1953), and that the minimum injection pressure to propagate them should be larger than the least principal stress (Hubbert and Willis 1957).

Based on this fundamental knowledge, Fig. 2a, b shows the expected orientation of hydraulic fractures relative to the orientation of the well. Figure 2a shows a case in which the least principal stress (σ_h in this example) is perpendicular to the axis of the well. In this case, hydraulic fractures propagate in a plane parallel to the axis of the well. Figure 2b shows the expected orientation of the hydraulic fractures when the least principal stress (σ_v in this example) is parallel to the axis of the well. In this case, hydraulic fractures propagate in a plane perpendicular to the well axis. It should be noted that, even though a vertical well is shown in Fig. 2a, b, the same reasoning applies for a horizontal (or lateral) well. These geometric observations are particularly relevant to the discussion presented in Sect. 5.

To estimate the fluid pressures necessary to propagate hydraulic fractures in the field, theoretical expressions have been derived. The relations derived by Hubbert and Willis (1957) and Haimson and Fairhurst (1967) are among the most accepted and used in practice. The expression proposed by Hubbert and Willis (1957) estimates the minimum fluid pressure (P_{HW}) necessary to "hold open and extend a fracture" and can be initially written as Eq. 1. This minimum fluid pressure corresponds to FPP in Fig. 1.

$$P_{HW} \cong \sigma'_{Min} + P_{initial} \tag{1}$$

In which σ'_{Min} is the least principal effective stress and $P_{initial}$ is the original pore pressure of the formation. Hubbert and Willis (1957) used this initial concept to derive an expression for a specific case of incipient normal faulting, in which the least principal effective stress is horizontal with a magnitude of, approximately, a third of the effective vertical stress:

$$\sigma'_{Min} = \sigma'_h \cong \frac{\sigma'_V}{3} = \frac{\left(S_V - P_{initial}\right)}{3} \tag{2}$$

In which S_V is the total vertical stress. Therefore, based on these reasoning and conditions, the minimum pressure to "hold open and extend a fracture" can be obtained from (1) and (2):

$$P_{HW} \cong \frac{\left(S_V + 2P_{initial}\right)}{3} \tag{3}$$

However, in the case considered, the least principal effective stress is horizontal and approximately the same as the effective vertical stress, then:

$$\sigma'_{Min} = \sigma'_h \cong \sigma'_V = \left(S_V - P_{initial}\right) \tag{4}$$

Which would result in:

$$P_{HW} \cong S_V \tag{5}$$

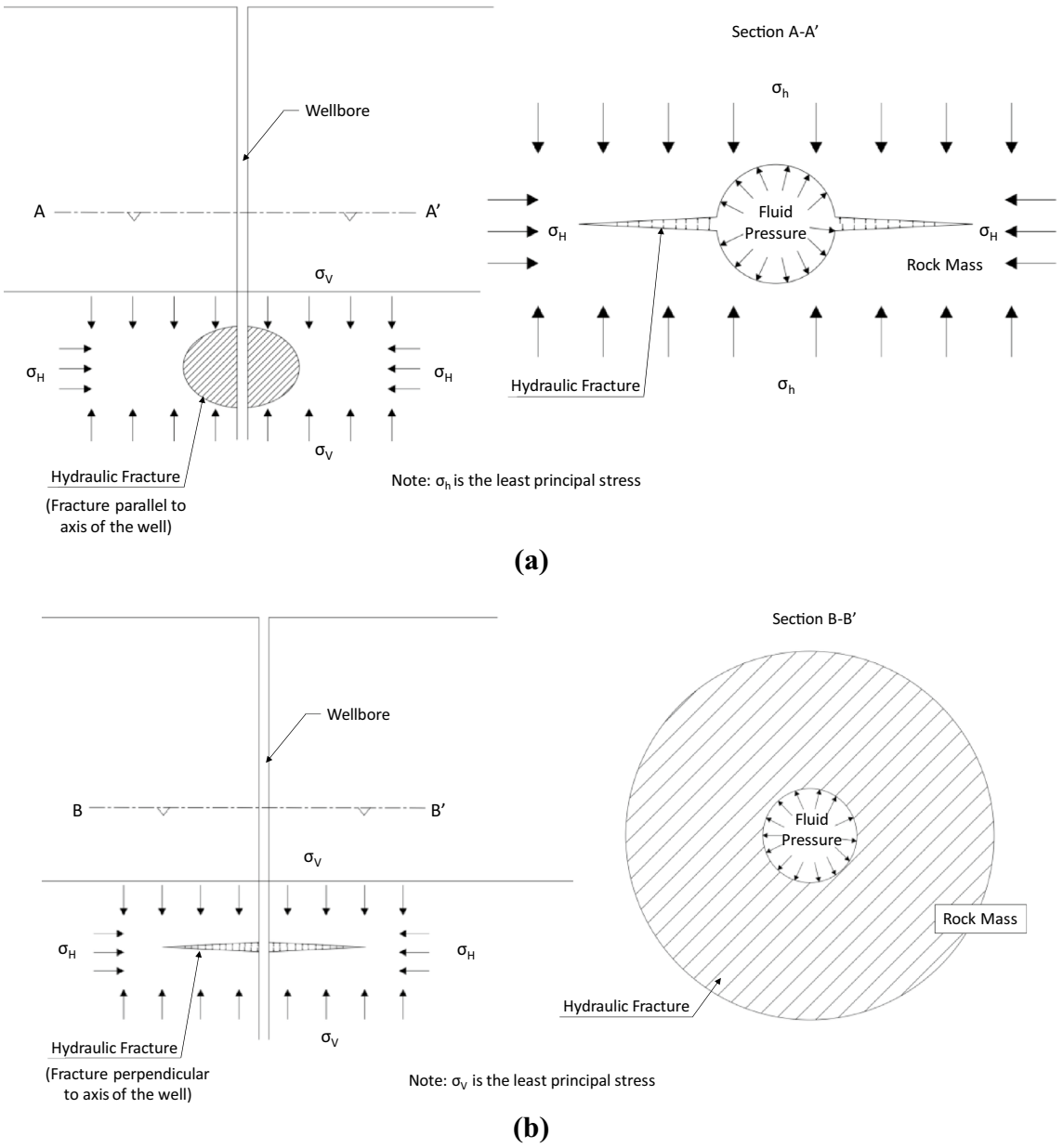

Fig. 2 Cross section of hydraulic fracture (**a**) parallel and (**b**) perpendicular to axis of wellbore

This clearly shows that, theoretically, the pressure necessary to hold and propagate a hydraulic fracture is significantly dependent on the in situ principal stresses, as intuitively expected.

Haimson and Fairhurst (1967), on the other hand, applied the criterion proposed by Hubbert and Willis (1957) to estimate the fracture initiation pressure, which corresponds to FIP in Fig. 1. This criterion assumed that a "crack would occur at a point of the boundary of the wellbore" where the tangential stress ($\sigma_{\theta\theta}$ in Fig. 3a) overcomes the tensile strength of the rock (σ_t), therefore, propagating parallel to the axis of the well as indicated in Fig. 3a. Since the stresses in the wall of a circular opening simultaneously subjected to far-field stresses and to an internal pressure are analytically known, the tangential stresses $\sigma_{\theta\theta}$ can be calculated as:

$$\sigma_{\theta\theta} = \left(S_{\mathrm{H}} + S_{\mathrm{h}} - P_{\mathrm{initial}}\right) - 2\left(S_{\mathrm{H}} - S_{\mathrm{h}}\right)\cos\left(2\theta\right) \tag{6}$$

In which S_{H} and S_{h} are the maximum and minimum in situ principal stresses, respectively, which are typically but not necessarily horizontal. For $\theta = 0^{\mathrm{o}}$ (see Fig. 3b), one obtains the maximum tangential stress as:

$$\sigma_{\theta\theta} = \left(3S_{\mathrm{h}} - S_{\mathrm{H}} - P_{\mathrm{initial}}\right) \tag{7}$$

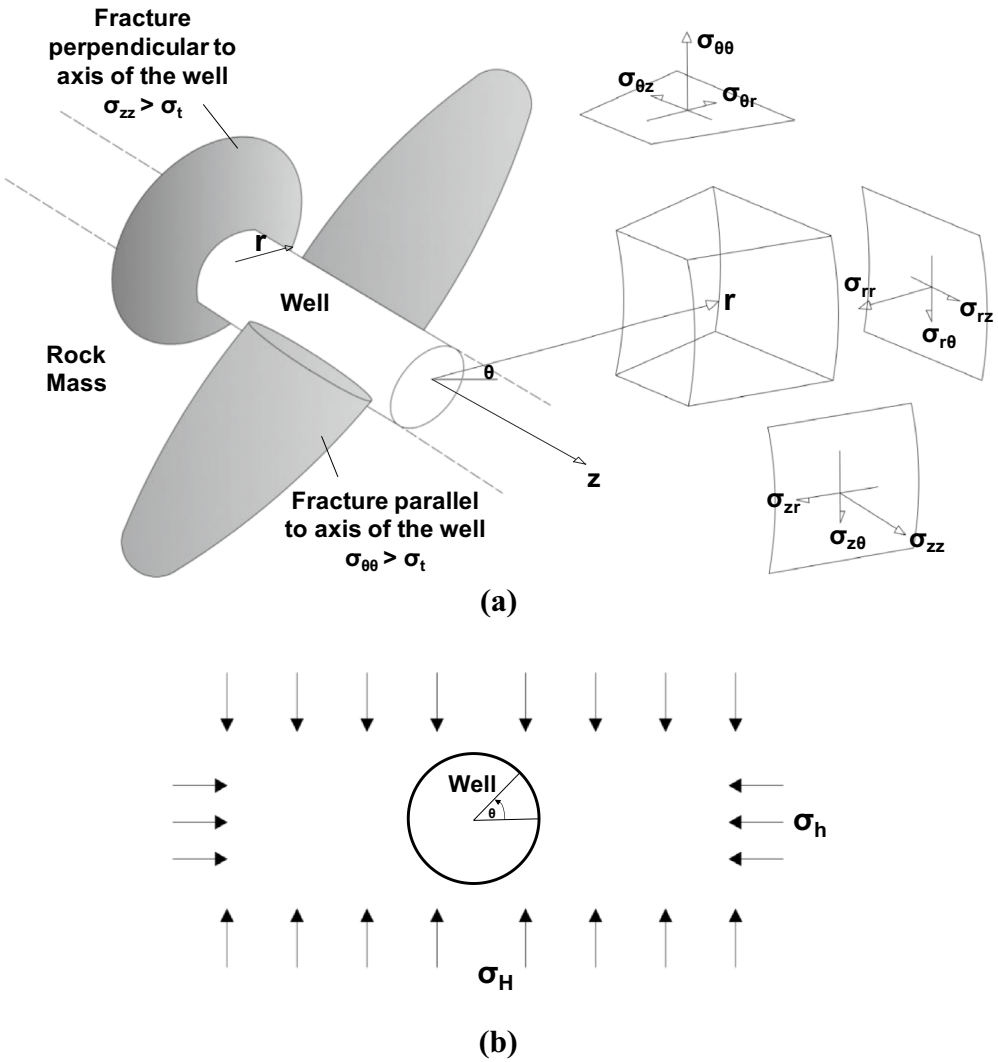

Fig. 3 **a** Stresses around a circular opening subjected to **b** biaxial loading conditions

This analytical solution led to the expression used in the ASTM D4645 (2004) as a standard method of estimating in situ rock stresses through the hydraulic fracturing of the rock. This method, proposed by Haimson and Fairhurst (1967), states that the fracture initiation pressure (identified as P_{HF} in this technical note, which corresponds to FIP in Fig. 1) needs to overcome the maximum tangential stress in the borehole and the tensile strength of the rock:

$$P_{HF} = \sigma_t + \sigma_{\theta\theta} \tag{8}$$

which, from Eqs. (7) and (8), can be further written as:

$$P_{HF} = \sigma_t + 3S_h - S_H - P_{initial} \tag{9}$$

which is valid if one considers no fluid penetration. If leakage and, therefore, fluid penetration take place, then poro-elasticity should be taken into account with parameter A:

$$P_{HF} = \sigma_t + \frac{\left(3S_h - S_H - P_{initial}\right)}{A} \tag{10}$$

where P_{HF} is the fracture initiation pressure at the bottom of the wellbore and σ_t is the tensile strength of the rock to be hydraulically fractured; as mentioned earlier, S_h and S_H are typically considered horizontal, but it is not uncommon that the vertical stress is smaller than both horizontal stresses, becoming, in this case, the minimum principal stress. $P_{initial}$ is the original formation pore pressure and $A = 2 - \alpha\frac{(1-2\nu)}{(1-\nu)}$, in which ν is the Poisson's ratio of the rock and α is the Biot poro-elastic parameter of rock (Haimson and Fairhurst 1967; Haimson and Zhao 1991).

While theoretical estimates of the expected breakdown pressures are typically carried out for hydraulic fracturing operations, there are limited studies (1) evaluating the

variation of the field breakdown pressures for different types of rock and depths, i.e., vertical stresses, and (2) comparing the field breakdown pressures with theoretical values. These aspects are addressed in this technical note.

3 Methodology

3.1 Data Collection and Assumptions

To evaluate the effect of the effective vertical stresses on the formation breakdown pressures, literature sources discussing several hydraulic stimulation projects in shale and EGS reservoirs were reviewed. It should be noted that gathering the relevant information of the analyzed projects is complex because the same project may include a number of stimulation wells. Therefore, in order to simplify the reading of the results, the location of the project and the well identification (if more than one well is considered) are documented in Tables 1 and 2. When not available in the literature used, the effective vertical stresses were estimated based on the following assumptions:

- An average unit weight of 23 kN/m^3 (148 pcf) for the rock and soil above the stimulated rock layer.
- Hydrostatic pore pressure and ground water level located at the surface.

Moreover, in some of the analyzed projects, only the well-head pressures were available. To obtain the bottom-hole pressures based on the well-head pressures, the variation of the injected fluid pressure p with depth z was initially calculated as follows:

$$\left(\frac{\mathrm{d}p}{\mathrm{d}z}\right) = \left(\frac{\mathrm{d}p}{\mathrm{d}z}\right)_{\mathrm{H}} + \left(\frac{\mathrm{d}p}{\mathrm{d}z}\right)_{\mathrm{F}} + \left(\frac{\mathrm{d}p}{\mathrm{d}z}\right)_{\mathrm{A}} \tag{11}$$

where $\left(\frac{\mathrm{d}p}{\mathrm{d}z}\right)$ is the total pressure gradient and $\left(\frac{\mathrm{d}p}{\mathrm{d}z}\right)_{\mathrm{H}}$, $\left(\frac{\mathrm{d}p}{\mathrm{d}z}\right)_{\mathrm{F}}$ and $\left(\frac{\mathrm{d}p}{\mathrm{d}z}\right)_{\mathrm{A}}$ are the hydrostatic, frictional and acceleration gradients, respectively. However, for the flow rate, well diameter and friction between fluid and well wall of a typical hydraulic fracturing project, the frictional and acceleration gradients are much smaller than the hydrostatic gradient. While the authors believe that it is important to note that these gradients exist, it is not in the scope of this technical note to calculate the three distinct gradients. Therefore, it is assumed that

$$\left(\frac{\mathrm{d}p}{\mathrm{d}z}\right) = \left(\frac{\mathrm{d}p}{\mathrm{d}z}\right)_{\mathrm{H}} = \rho g \tag{12}$$

which translates into

$$p_{bottom-hole} = p_{well-head} + \rho g z \tag{13}$$

where ρ is the density of fracturing fluid (assumed 1000 kg/m^3), g is the acceleration of gravity (assumed 10 m/s^2), and z is the depth of interest (m).

Since some of the data that will be analyzed and discussed in Sects. 4 and 5 are based on the assumptions presented in this subsection, the overall data are, therefore, semi-empirical. However, one must emphasize that the assumptions related to the unit weight and pressure gradients explained earlier are realistic and theoretically supported, which therefore result in reliable estimates of effective vertical stresses and formation breakdown pressures.

3.2 Projects Analyzed

The analyzed hydraulic fracturing well stimulations included shale oil and/or gas, as well as EGS projects, as illustrated in Figs. 4 and 5, respectively. The locations of the wells analyzed in this technical note are represented by the black circles in Figs. 4 and 5. The highlighted areas in Fig. 4 are the analyzed shale oil and gas plays according to the U.S. Energy Information Administration (2011).

The rock formations used in the shale oil/gas and EGS projects will now be briefly described:

- Shale oil and/or gas
  - Barnett Shale:
    The Barnett Shale formation consists of sedimentary rocks that can be encountered in the Fort Worth Basin in north-central Texas. Currently, the production is limited to the northern basin where the Barnett Shale is relatively thick (> 92 m) (Montgomery et al. 2005). Lithologically the formation consists of black siliceous shale, limestone, and minor dolomite (Konstantinos 2005). Most fractures appeared to have developed in opening-mode (Gale et al. 2007) and are highly clustered. Also, the in situ stress S_{Hmax} trends northeast–southwest in the Fort Worth Basin. The well considered in this study is located north of Fort Worth, Texas, was stimulated in 2000, and has a depth of 2169 m (Siebrits et al. 2000).
  - Woodford Shale
    The Woodford Shale formation is located in northwest Oklahoma. The depth of the Woodford Shale varies between 1830 and 3660 m with a thickness between 15 and 90 m. The analyzed well was stimulated in 2013 and has a depth of 2215 m (French et al. 2014). Badra (2011) pointed out that there are abundant natural fractures perpendicular to the bedding planes.
  - Haynesville Shale
    This sedimentary depositional area characterized by different mudrock lithologies has a depth of more

Table 1 Summary of the effective vertical stresses (σ_v') and bottom-hole breakdown ($P_{breakdown}$) pressures in the analyzed shale oil and/or gas projects

	Shale oil and/or gas Project									
	Barnett shale Siebrits et al. (2000)	Woodford shale French et al. (2014)	Haynesville shale Fonseca and Farinas (2013)	Bakken shale Phillips et al. (2007)	Marcellus Shale					Antrim shale Hopkins et al. (1998)
Location	Texas	Oklahoma	Western louisiana	North dakota	Tioga county, PA Mayerhofer et al. (2011)	Potter county, PA Fontaine et al. (2008)	Greene County, PA (Yeager and Meyer 2010)			Michigan
							Well A	Well B	Well C	
Depth (m)	2169	2215	3738	3034	1820	1600	2479	2445	2553	364
Lithology	Calcic-siliceous shale, calcareous mudstone	Siliceous shale	Mudrocks	Argillaceous dolostones and siltstones	Thinly laminated non-calcareous fissile pyritic organic-rich shale					Shale interbedded with carbonate
Fractures/Faults	Opening-mode fractures	Natural fractures are perpendicular to the bedding planes	Many of the natural fractures are sealed by cementitious materials	Direction of natural fractures is N35°E	Two vertical fracture sets (or joints) are present in the Marcellus Shale: J1 and J2. J1 fractures are oriented NE-SW. J2 fractures are oriented NW–SE					Two primary fracture sets: one striking NW–SE and the other NE-SW
In situ stresses (when available)	S_H trends NE-SW	N/A	N/A	S_H trends N68°E	N/A					N/A
Effective vertical stress—σ_v' (MPa)	28*	29*	49*	39*	24*	21*	22	22	25	5*
Bottom-hole breakdown Pressure—$P_{breakdown}$ (MPa)	52	55**	90	75**	70**	59**	55	52	55	22
Ratio of $P_{breakdown}/\sigma_v'$	1.86	1.92	1.85	1.92	2.92	2.81	2.50	2.36	2.20	4.40

*Denotes effective vertical stresses calculated using the methodology described in Sect. 3.1

**Denotes bottom-hole breakdown pressures calculated using the methodology described in Sect. 3.1

Table 2 Summary of the effective vertical stresses (σ_v') and bottom-hole breakdown ($P_{breakdown}$) pressures in the analyzed EGS projects

	EGS project							
	Cooper basin	Basel 1 Baisch and Voros (2009)	Fjällbacka (Fjb1) McClure and Horne, (2014)	Ogachi (OGC 1)	GeneSys	KTB,1994 Baisch and Voros (2009)	Fenton Hill,	Soultz GPK4
Location	Australia	Switzerland	Sweden	Japan	Germany	Germany	New Mexico, USA	France
Depth (m)	4135	4400	445	1000 Kaieda et al. (2010)	3900 Tischner et al. (2013)	9100	3500 Brown et al. (2012)	4700 Charléty et al. (2007)
Lithology	Granitic basement	Crystalline basement (mainly, granitoid rocks > 99%)	Granitic basement	Cretaceous granodiorite basement	Sandstones, siltstones and claystones	Metamorphic basement rocks with granitic intrusions	Biotite granodiorite basement	Granitic basement
Fractures/Faults	Dominant fault and fracture networks trend NW–SE and NE–SW	Dominant natural fracture set strikes NW–SE to NNW–SSE	Subvertical natural fracture sets striking NW and NE	Natural fractures with average spacing of about 8 cm	15 km long sub vertical fault striking NEE–SWW	Most faults follow the foliation and dip either to SW or to NE	Natural fractures are sealed with secondary minerals	The average strike direction is $N160^{\circ}E \pm 15^{\circ}$
In situ Stresses	In situ stress magnitudes estimated as $S_H/S_h/\sigma_V \cong 1.3/1.2/1.0$	In situ stress state $S_H > \sigma_V > S_h$	The vertical stress is the minimum stress down to a depth of about 450-500 m	In situ stress state is $S_H > \sigma_V > S_h$	The minimum horizontal principal stress is about 90% of the overburden	In situ stress state is $S_H > \sigma_V > S_h$	In situ stress magnitudes estimated as $S_H/S_h/\sigma_V \cong 0.7/0.6/1.0$	In situ stress magnitudes estimated as $S_H/S_h/\sigma_V \cong 1.05/0.58/1.0$
Effective vertical stress—σ_v' (MPa)	21 Shen (2008) Note: Overpressurized pore fluid	66 Häring et al. (2008)	6*	13*	51*	118*	58 Fehler (1989)	72 Valley and Evans (2007)
Bottom-hole breakdown Pressure—$P_{breakdown}$ (MPa)	104 McClure and Horne (2014)	74**	20	28 McClure and Horne, (2014)	72** Baisch and Voros, (2009)	144	67** Brown (2009)	64** Baisch and Voros (2009)
Ratio of $P_{breakdown}/\sigma_v'$	4.95	1.13	3.33	2.15	1.44	1.22	1.15	0.90

*Denotes effective vertical stresses calculated using the methodology described in Sect. 3.1

**Denotes bottom-hole breakdown pressures calculated using the methodology described in Sect. 3.1

Fig. 4 Locations of the analyzed shale oil and/or gas hydraulic stimulations in the United States

than 3050 m and is located in northwestern Louisiana, southwestern Arkansas and eastern Texas. Its thickness varies between 60 and 90 m. Nunn (2012) noted that the visual inspection of the cores from the formation revealed numerous fractures, many of which had been resealed by cement indicating that they occurred by natural processes. In the context of this technical note, a 3732 m-deep well stimulated in 2010 and located in northwestern Louisiana was analyzed (Fonseca and Farinas 2013).

– Bakken Shale

This formation spreads throughout the subsurface of the Williston Basin, underlying parts of Montana, North Dakota, Saskatchewan and Manitoba (Wang and Zeng 2011). Lithologies vary from argillaceous dolostones and siltstones to clean, quartz-rich arenites and oolitic limestones (Cramer 1986, Breit et al. 1992). Kuhlman et al. (1992) concluded that the direction of maximum horizontal stress was N67.6°E and the natural fracture direction was predominately

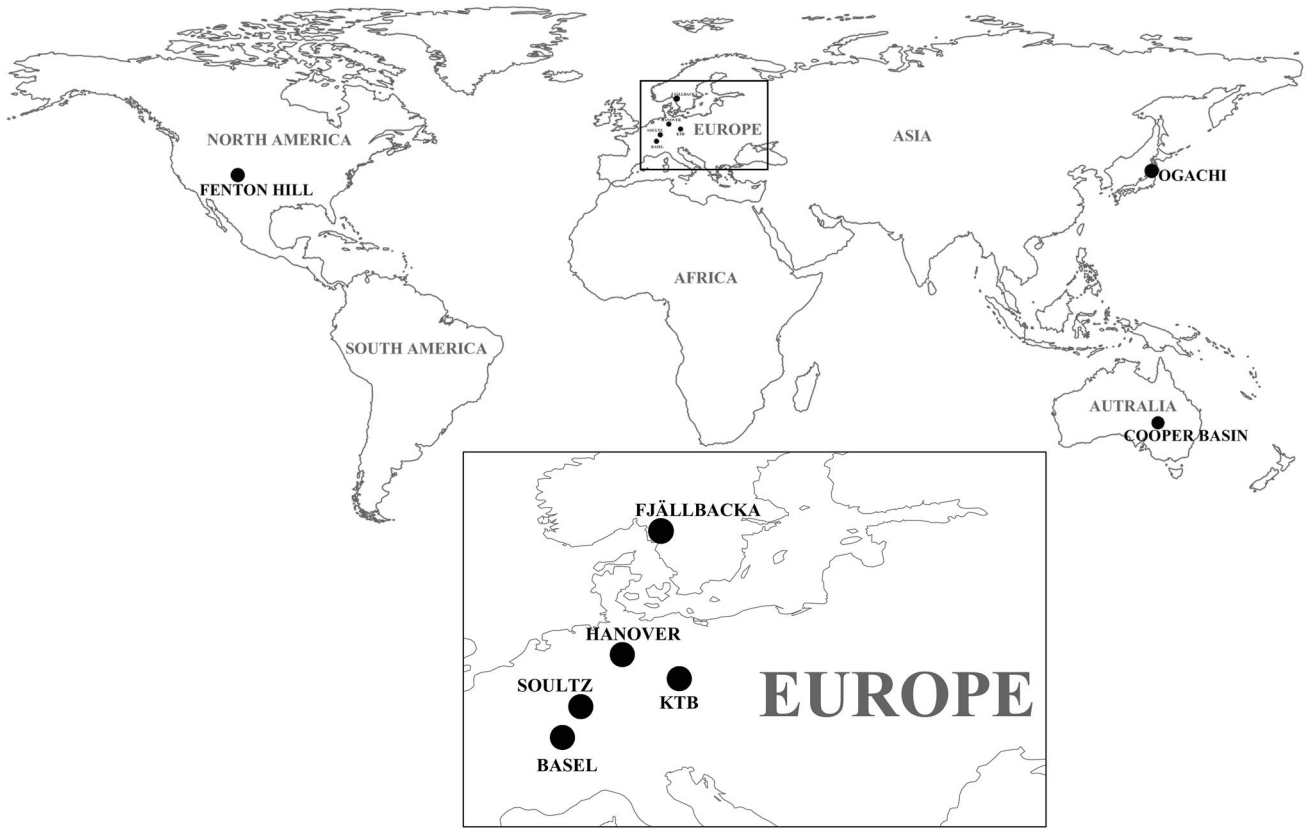

Fig. 5 Locations of the analyzed EGS projects

N35°E. In this technical note, a well with a depth of 3034 m located in North Dakota was analyzed. The stimulation of the well took place between 2005 and 2006 (Phillips et al. 2007).

– Marcellus Shale

The Marcellus shale formation spreads throughout a large area (more than 233,000 km^2) in the northeastern of the United States. Preliminary estimates reveal that this formation could be the world's largest natural gas field with over 14 trillion cubic meters of gas (Engelder et al. 2009). The formation is predominantly composed of gray-black to black thinly laminated non-calcareous fissile pyritic organic-rich shale (Matthew et al. 2009), underpressurized to the southwest and normal to potentially overpressurized to the northeast (Zagorski et al. 2012). For this analysis, three wells located in northwest and central Pennsylvania were considered. These stimulations took place in 2009, 2007 and 2010 in Tioga, Potter and Greene counties, respectively.

– Antrim Shale

The Antrim shale is part of a large Devonian black shale system which extends across most of the eastern cratonic region of North America with depths varying between 152 and 700 m. An important feature of the Antrim Shale formation is the presence of two primary fracture sets: one striking northwest–southeast and the other northeast–southwest (Ryder 1990), with fracture spacing ranging between 0.2 and 2.0 m (Richards et al. 1994). A well located in the Montmorency county of Michigan with a depth of 364 m and stimulated in 1993 (Hopkins et al. 1998) is used for this analysis.

- Engineered Geothermal Systems

  – Cooper Basin

  The Cooper Basin is the largest onshore petroleum province in Australia and has both conventional and unconventional reservoirs (Hill and Gravestock 1995). This EGS project is located in the northeast of South Australia near Moomba and is characterized by a granite basement overlain by approximately 3600 m of sedimentary cover. Also, this granitic basement is saturated with brine, which is regionally pressurized at ~ 34.4 MPa above the hydrostatic pressure. In the project area, the maximum horizontal rock stress is orientated east–west due to tectonic compression of the Australian plate with the in situ

stress magnitudes estimated as $S_H/S_h/\sigma_V \cong 1.3/1.2/1.0$ (Shen 2008). The selected well has an approximate depth of 4135 m and a static rock temperature at the bottom of the wellbore of 250 °C. The stimulation of the well took place in 2003 (Wyborn et al. 2005).

– Basel

This geothermal project was located in the city of Basel, Switzerland. The crystalline basement (primary basement rock types include granitoid rocks (> 99%), aplite and lamprophyre) of the formation is covered by sedimentary rocks with a combined thickness of 2507 m (Ziegler et al. 2015). The dominant natural fracture set strikes NW–SE to NNW–SSE, with steep dips exceeding 60°. In this study, the stimulation of Basel 1, a near-vertical well, is considered. The analyses of the borehole breakouts indicate that the least principal in situ stress S_h is oriented along an azimuth of $54 \pm 14^{\circ}$ and that $S_H > \sigma_V > S_h$ (Valley and Evans 2007). The estimated reservoir temperature at a final depth of 4400 m was 190 °C. The stimulation treatment of the Basel 1 took place in 2006 (Häring et al. 2008).

– Fjällbacka

Fjällbacka is a Swedish heat pump project, in which hydraulic fracturing was used to stimulate the rock. It is located in the central part of the Bohus granite massif, south of the village Fjällbacka, on the west coast of Sweden (Jupe et al. 1992). The majority of the bedrock in this region belongs to crystalline Precambrian with a low natural permeability and low heat flow density with temperature gradients in the range of 10–18 °C/km. Given the low temperature gradients, heat pumps were used to elevate the fluid temperatures to levels suitable to local heating purposes (Doherty et al. 1994). The approximate depth of the well is 445 m and its stimulation took place in 1986 (Wallroth et al. 1999). The fracture pattern, dominated by two almost orthogonal vertical/subvertical sets (striking NW and NE, respectively) and one horizontal/subhorizontal set, creates an almost cubic pattern of blocks (Eliasson et al. 1988). The minimum principal stress appears to be vertical down to a depth of about 450–500 m, thereby favoring the opening of horizontal fractures during fluid injections. The largest horizontal principal stress strikes approximately NW–SE, as commonly observed in western Sweden (Wallroth, 1990).

– Ogachi

The Ogachi site is located in the volcanic crater of northern Japan. The geology of the site comprises a cover of Tertiary lapilli tuff to a depth of 300 m from the surface and a basement rock of Cretaceous granodiorite. The average spacing of the natural fractures in the granodiorite is about 8 cm, as observed from geological investigations (Kitano et al. 2000). The magnitudes of the in situ stresses at the reservoir are estimated as $S_H = 30 \sim 40$, $S_h \sim 22$ and $\sigma_v \sim 25$ MPa (Shin et al. 2000). The depth of the well is 1000 m with an approximate temperature of 230 °C at its bottom. The stimulation of the well took place in 1992 (Kaieda et al. 2010).

– GeneSys

The GeneSys (Generated geothermal energy Systems) project is located in Hanover, Germany. The local stratigraphy consists of tight sedimentary rocks formed by alternating layers of fine-grained sandstones, siltstones and claystones. The minimum principal stress (σ_h) is about 90% of the overburden (Jung et al. 2005). A temperature of 169 °C was encountered at the final depth of 3901 m of the analyzed well. Its stimulation took place in 2011 (Tischner et al. 2013).

– KTB

The Kontinentale Tiefbohrung (KTB) geothermal project is located in Southeastern Germany near the western margin of the Bohemian Massif (Wagner et al. 1997). The Bohemian Massif is composed of medium- to high-grade metamorphic basement rocks with granitic intrusions (O'Brien et al. 1997). Most faults follow the foliation and dip 50–80° either to SW or to NE and strike approximately NW–SE (Hirschmann et al. 2006; Wagner et al. 1997). Brudy et al. (1997) showed that the profile of the stress magnitudes below 1 km depth suggests that $S_H > \sigma_v > S_h$, which indicates a strike-slip regime. Additionally, the orientation of the S_H is found to vary between N150°E and N170°E along the depth of the investigated interval from 3.2 to 8.6 km depth. A temperature of 270 °C was reached at the final depth of 9100 m of the analyzed well, which was stimulated in 2000 (Jost et al. 1998).

– Fenton Hill

The Fenton Hill EGS site is located in the Jemez Mountains of north-central New Mexico, about 32 km west of Los Alamos. The rock formation at Fenton Hill is a homogeneous biotite granodiorite body with very low permeability. Even though natural fractures are present, they are characteristically sealed with secondary minerals (Laughlin et al. 1983). Zoback et al. (1985) concluded that the minimum stress is horizontal (S_h) and oriented N104°E, and the maximum in situ stress is vertical, with $S_H/S_h/\sigma_v = 0.7/0.6/1$. The temperature at the final depth of 3500 m was 235 °C. The stimulation of the analyzed well took place between 1986 and 1995 (Brown 2009).

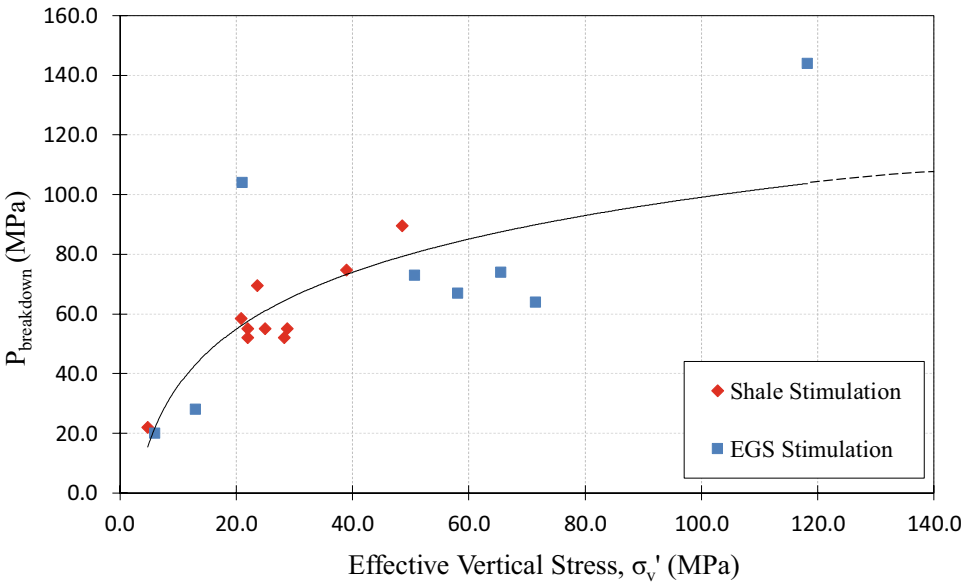

Fig. 6 Variation of $P_{breakdown}$ in shale oil and/or gas and EGS projects with the vertical effective stresses. The black line intends to show a trend rather than providing a statistical relationship between the variables

– Soultz (GPK4)

The site is located in Soultz-sous-Forêts, France, where the stimulations of GPK1, GPK2, GPK3 and GPK4 geothermal wells were conducted. The high temperatures found in this area occur due to the groundwater circulation in fractures distributed in the Cenozoic and Mesozoic sedimentary cover, which are connected to fractures within the Paleozoic granitic basement (Charléty et al. 2007). Valley and Evans (2007) concluded that the orientation of the maximum horizontal stress (S_H) is N169°E ± 14° whereas the relative magnitudes of the principal in situ stresses are estimated as $S_H/S_h/\sigma_v = 1.05/0.58/1$. This analysis focused on the stimulation of GPK4, which took place in 2005. The temperature was approximately 200 °C at a depth of 4700 m (Vidal et al. 2015).

4 Results

4.1 Field Observations

Tables 1 and 2 show the stimulation data of ten and eight shale oil and/or gas and EGS projects, respectively. The collected and investigated data include (1) the depths to the bottom of the well, (2) the effective vertical stresses σ'_v, (3) the bottom-hole breakdown pressures ($P_{breakdown}$) and (4) the ratio between the breakdown pressures and the effective vertical stresses $\left(\frac{P_{breakdown}}{\sigma'_v}\right)$.

From the analyzed projects, it can be noted that the shallowest shale oil and/or gas project is the stimulation of the Antrim shale formation with a depth of 364 m and a breakdown pressure of 22 MPa. The deepest project is the stimulation of the Haynesville shale formation with a depth of 3738 m and a breakdown pressure of 90 MPa. These stimulations correspond to a ratio of $\left(\frac{P_{breakdown}}{\sigma'_v}\right)$ of 4.40 for the Antrim shale and 1.28 for the Haynesville shale formation. Similarly, the shallowest EGS project analyzed is the Fjällbacka well in Sweden (used for a heat pump rather than EGS) with a depth of 445 m and a breakdown pressure of 20 MPa, while the deepest EGS project is the stimulation of the Kontinentale Tiefbohrung (KTB) geothermal project in Germany with a depth of 9100 m and a bottom-hole breakdown pressure of 144 MPa. A $\left(\frac{P_{breakdown}}{\sigma'_v}\right)$ ratio of 3.33 is obtained for the Fjällbacka well whereas for the KTB project this ratio is 1.22. It seems evident that $P_{breakdown}$ increases and the ratio of $\left(\frac{P_{breakdown}}{\sigma'_v}\right)$ decreases as the effective vertical stress increases, for both shale oil and/or gas and EGS stimulations.

The results shown in Tables 1 and 2 are plotted in Figs. 6 and 7, which depict the variation of the effective vertical stresses with $P_{breakdown}$ and with the ratio of $\left(\frac{P_{breakdown}}{\sigma'_v}\right)$ for the analyzed projects.

From this analysis, it is clear that there is a strong relation between the effective vertical stresses and the bottom-hole breakdown pressures, regardless of the type of stimulation, e.g., shale oil and/or gas or EGS. As the effective vertical stresses increase, the breakdown pressures also increase, as intuitively expected. Furthermore, as the vertical effective stress increases, the ratio $\left(\frac{P_{breakdown}}{\sigma'_v}\right)$ seems to approach 1.0,

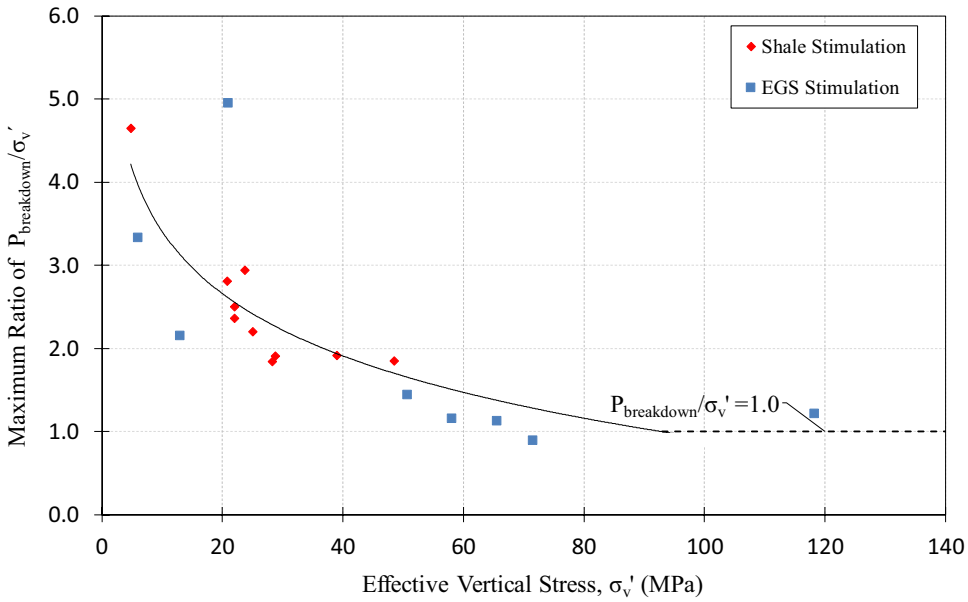

Fig. 7 Variation of the ratio $P_{\text{breakdown}}/\sigma_v'$ in shale oil and/or gas and EGS projects with the vertical effective stresses. Note: the black line intends to show a trend rather than providing a statistical relationship between the variables

which indicates that the breakdown pressure is systematically larger than or equal to the vertical effective stress. It should be noted that this is concluded based on the data analyzed in the current study. These data are very protected by operators and are, frequently, not made public. While more data would ideally need to be analyzed to confirm this observation (i.e., that the breakdown pressure is systematically larger than or equal to the vertical effective stress), possible reasons for it will be discussed in Sect. 5.

Furthermore, for deep formations (σ_v'>50MPa), the bottom-hole breakdown pressures are only slightly higher than the effective vertical stresses $\left(1.0 < \frac{P_{\text{breakdown}}}{\sigma_v'} < 1.5\right)$, while for shallower formations ($\sigma_v' < 50$MPa) the bottom-hole breakdown pressures are significantly higher than the effective vertical stress $\left(1.5 < \frac{P_{\text{breakdown}}}{\sigma_v'} < 5.0\right)$.

4.2 Comparison Between Field Observations and Theoretical Models

It is important to investigate how the field data fit into the theoretical models derived by Hubbert and Willis (1957) and Haimson and Fairhurst (1967) discussed in Sect. 2. Six shale oil and/or gas and EGS stimulation projects were selected (Table 3) where the minimum and maximum horizontal stresses, as well as tensile strength of the reservoir rock, were published in the literature. Equation 1 was used when applying the methodology proposed by Hubbert and Willis (1957) to estimate the minimum pressure to "hold open and extend a fracture" (P_{HW}), since it considers a general state of stress as opposed to Eq. 3. Equation 10 was used to estimate the fracture initiation pressures (P_{HF}) for the relationship developed by Haimson and Fairhurst (1967). This equation requires the calculation of parameter A, which depends on the Poisson's ratio and the Biot poro-elastic parameter of rock (α). Based on the literature values, the Poisson's ratio was assumed to vary between 0.2 and 0.35 for the oil and gas projects (Agapito and Hardy 1982) (sedimentary rocks, usually shale) and between 0.23 and 0.28 for the EGS projects (Detournay and Cheng 1993; Xin 2014) (crystalline rocks, usually granitic); the Biot's poro-elastic parameter was assumed to vary between 0.75 and 0.80 for the oil and gas projects (Gray 2017) and between 0.3 and 0.35 for the EGS projects (Berryman 2005; Detournay and Cheng 1993). Moreover, two "fluid infiltration" conditions were considered: "no fluid infiltration", which may be realistic if the injection rate is very high, for example, resulting in $A=1$, and "fluid infiltration", which results in $A=f(\nu, \alpha)>1$. Based on the parameters and conditions considered, a range of possible P_{HF} values were obtained. Figures 8 and 9 illustrate the field and theoretical fracturing pressures and the ratio of $\frac{P_{\text{breakdown/HW/HF}}}{\sigma_v'}$ versus the effective vertical stress in various shale oil and/or gas and EGS projects, respectively. Examples of calculation of P_{HW} using Hubbert and Willis (1957) and P_{HF} using Haimson and Fairhurst (1967) are given based on the in situ stresses shown in Table 3.

- Example of calculation for Hubbert and Willis (1957) model for the Marcellus shale well analyzed:

Equation 1:

$$P_{\text{HW}} \cong \sigma'_{\text{Min}} + P_{\text{initial}}$$

$$\sigma'_{\text{Min}} = S_h - P_{\text{initial}} = 41 - 23 = 18\text{MPa}$$

$$P_{\text{initial}} = 23\text{MPa}$$

Table 3 Field and theoretical pressures and $\frac{P_{breakdown/Min/HF}}{\sigma_v'}$ in different shale oil and/or gas and EGS projects

Project and location	Depth (m)	Total Vertical Stress—σ_v (MPa)	Pore Pressure (MPa)	Tensile strength of Rock (MPa)	Orientation of the well	Max. Horizontal stress—S_H (MPa)	Min. Horizontal stress—S_h(MPa)	Bottom-hole Pressure - $P_{breakdown/HW/HF}$ (MPa)			$P_{breakdown/HW/HF}/\sigma_v'$		
								From the Field (Tables 1 and 2)—$P_{breakdown}$	Hubbert and Willis (1957) P_{HW}	Haimson and Fairhurst (1967) P_{HF}	From the Field (Tables 1 and 2)—$P_{breakdown}$	Hubbert and Willis (1957) P_{HW}/σ_v'	Haimson and Fairhurst (1967) P_{HF}/σ_v'
Bakken Shale, North Dakota	3034	68.4	29.6	8.23 (Kuhlman et al. 1992)	Horizontal (Charles et al. 2004)	62 (Kuhlman et al. 1992)	55	75	55	48–82	1.92	1.41	1.24–2.11
Marcellus Shale- Well A, Greene County, PA	2479	45.0	23.0	7.63 (Jin et al. 2017)	Horizontal (Yeager and Meyer 2010)	48 (Yeager and Meyer 2010)	41	55	41	39–59	2.50	1.86	1.77–2.68
Cooper Basin, Australia	4135	96.0	75.0	12.5 (You 2015)	Vertical (Bendall et al. 2014)	136 (Shen 2008)	132	104	96	75–118	4.95	4.57	3.57–5.62
Soultz GPK4, France	4700	118.6	47.0		Semi-vertical (Dezayes et al. 2005)	107 (Valley and Evans 2007)	64	64	64	36–51	0.90	0.89	0.50–0.71
Fenton Hill, New Mexico	3500	92.8	34.7		Semi-vertical (Grigsby and Tester 1989)	65 (Fehler 1989)	56	67	56	55–81	1.15	0.96	0.95–1.39
Basel 1 Switzerland	4400	109.6	44.0		Vertical (Häring et al. 2008)	140 (Häring et al. 2008)	70	74	70	29–39	1.13	1.07	0.44–0.59

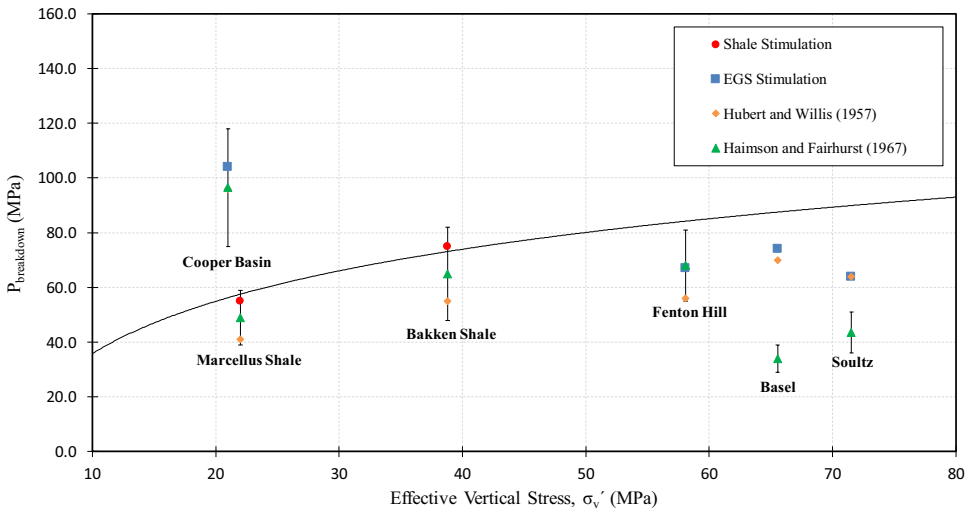

Fig. 8 Comparison between $P_{\text{breakdown}}$ in shale oil and/or gas and EGS projects, P_{HW} for Hubbert and Willis (1957) and P_{HF} for Haimson and Fairhurst (1967). The error bars represent the range of values obtained using the Haimson and Fairhurst (1967) approach

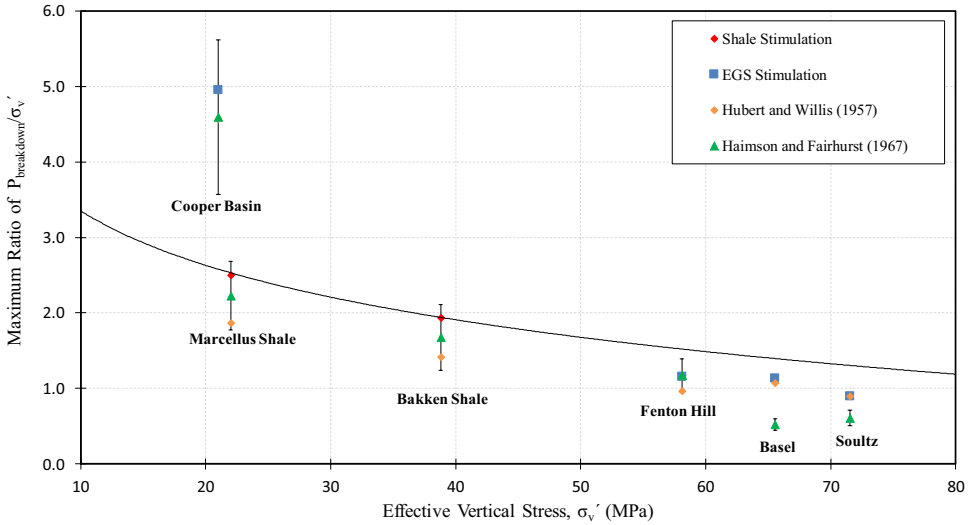

Fig. 9 Comparison between the ratio of $P_{\text{Breakdown}}/\sigma'_v$ in shale oil and/or gas and EGS projects, P_{HW} for Hubbert and Willis (1957) and P_{HF} for Haimson and Fairhurst (1967). Note: The error bars represent the range of values obtained using the Haimson and Fairhurst (1967) approach

$$P_{\text{HW}} \cong 18 + 23 = 41\text{MPa}$$

- Example of calculation for Haimson and Fairhurst (1967) for the Marcellus shale well analyzed:

No fluid infiltration:
Equation 9:

$$P_{\text{HF}} = \sigma_{\text{t}} + 3S_{\text{h}} - S_{\text{H}} - P_{\text{initial}}$$

$$P_{\text{HF}} = 7.6 + 3 \cdot 41 - 48 - 23 = 59\text{MPa}$$

Fluid infiltration:
Equation 10:

$$P_{\text{HF}} = \sigma_{\text{t}} + \frac{\left(3S_{\text{h}} - S_{\text{H}} - P_{\text{initial}}\right)}{A}$$

$$A = 2 - \alpha\frac{(1-2\nu)}{(1-\nu)}, \text{ with } \alpha = 0.75 \text{ and } \nu = 0.35,\ A = 1.654$$

$$P_{\text{HF}} = 7.6 + \frac{(3 \cdot 41 - 48 - 23)}{1.654} = 39\text{MPa}$$

Therefore, for this theoretical model: $39\text{MPa} < P_{\text{HF}} < 59\text{MPa}$.

The same procedure described above is used to calculate the P_{HW} for Hubbert and Willis (1957) and P_{HF} for Haimson and Fairhurst (1967), as shown in Fig. 8 for the Marcellus and Bakken shales, and for the Cooper Basin, Fenton Hill, Basel and Soultz EGS developments. The error bars in Haimson and Fairhurst (1967) account for the two scenarios of: "no fluid infiltration" and "fluid infiltration", in which the triangle represents the midpoint of the range obtained. For the Marcellus shale example, P_{HF} ranges between 39 and 59 MPa and the midpoint is 49 MPa.

In general, the theoretical models yield $P_{\text{HW/HF}}$ and $\frac{P_{\text{HW/HF}}}{\sigma'_v}$ ratios comparable to $P_{\text{breakdown}}$ and $\frac{P_{\text{breakdown}}}{\sigma'_v}$ obtained for shale oil and/or gas and EGS stimulation projects. Therefore, both

models appear to estimate $P_{\text{breakdown}}$ reasonably well for the analyzed hydraulic fracturing projects, with the exception of the Basel and Soultz projects, in which the Hubbert and Willis (1957) model showed better agreement with the field values. These differences will be discussed in Sect. 5.2.

5 Discussion

A theoretical interpretation of the variation of the field breakdown pressures with depth illustrated in Figs. 6 and 7 will initially be given using the approaches by Haimson and Fairhurst (1967) and Hubbert and Willis (1957). Subsequently, the differences between the field observations and the two theoretical methods, illustrated in Figs. 8 and 9, will be physically interpreted.

5.1 Variation of the Breakdown Pressure ($P_{\text{breakdown}}$) in the Field

Interpretation of results based on Hubbert and Willis (1957).

For shallow depths z—and consequently low vertical effective stresses—the field results show that the pressure necessary to propagate hydraulic fractures tends to a small value (Fig. 6), even though this pressure is always larger than the vertical effective stresses, as shown by the increase of $\frac{P_{\text{breakdown}}}{\sigma'_v}$ for low vertical effective stresses in Fig. 7. Based on Hubbert and Willis (1957), one can use Eq. 1 to calculate the limit of P_{HW} when the depth z tends to 0, as shown in Eq. 14, which indicates that P_{HW} theoretically tends, indeed, to a small value. However, it should be noted that, since this approach considers that the fracture already exists, the tensile strength of the rock is not considered in the calculation. This is the reason why P_{HW} tends to 0 and not to the tensile strength of the rock, as intuitively one may have expected.

$$\lim_{z\to 0} P_{\text{HW}} = \lim_{z\to 0}\left[\sigma'_{\text{Min}}(z) + P_{\text{initial}}\right] = 0 \tag{14}$$

As also seen in Fig. 6, as the vertical effective stress increases—or as the depth z increases—P_{HW} tends to infinity, since the trend line shown in the Fig. 6 continues to increase as the effective vertical stresses increase. Hubbert and Willis's approach also captures this trend, as shown in Eq. 15.

$$\lim_{z\to \infty} P_{\text{HW}} = \lim_{z\to \infty}\left[\sigma'_V(z) + P_{\text{initial}}(z)\right] = \infty \tag{15}$$

The variation of the field $P_{\text{breakdown}}$ normalized by the vertical effective stress σ'_V is also shown in Fig. 7. One of the main observations from the field data is that $\frac{P_{\text{Breakdown}}}{\sigma'_V}$ appears to tend to 1.0 for large depths, i.e., larger vertical effective stresses. Using Hubbert and Willis for two distinct but typical in situ stress conditions, one can note that $\frac{P_{\text{HW}}}{\sigma'_V} \approx 1.8$ for $\sigma'_{\text{Min}} = \sigma'_{\text{V}}$ (Eq. 16) and that $\frac{P_{\text{HW}}}{\sigma'_V} \approx 0.9$ for $\sigma'_{\text{Min}} = \frac{\sigma'_V}{2}$ (Eq. 17). These values were obtained using an estimate for the rock and water densities of 23kN/m^3 and 10kN/m^3, respectively. More intuitively, these results show that when $\sigma'_{\text{Min}} = \sigma'_{\text{V}}$, one needs to apply 1.8 times the effective vertical stress to hold open and propagate a fracture; this value decreases to a half if σ'_{Min} is also a half of the vertical effective stress. This may explain why it is not common to obtain $\frac{P_{\text{HW}}}{\sigma'_{\text{V}}}$ (or, as expressed for the field data in this study, $\frac{P_{\text{breakdown}}}{\sigma'_{\text{V}}}$) in the field that is very different from 1.0 at greater depths.

$$\begin{aligned}\lim_{z\to \infty} \frac{P_{\text{HW}}}{\sigma'_{\text{V}}} &= \lim_{z\to \infty}\left[\frac{\sigma'_{\text{V}}(z) + P_{\text{initial}}(z)}{\sigma'_{\text{V}}(z)}\right] \\ &= \lim_{z\to \infty}\left[\frac{\sigma_{\text{V}}(z)}{\sigma'_{\text{V}}(z)}\right] = \lim_{z\to \infty}\left[\frac{\gamma_{\text{Rock}}\cdot z}{\left(\gamma_{\text{Rock}} - \gamma_{\text{Water}}\right)\cdot z}\right] \\ &= \frac{23}{23-10} = 1.8\end{aligned} \tag{16}$$

$$\begin{aligned}\lim_{z\to \infty} \frac{P_{\text{HW}}}{\sigma'_{\text{V}}} &= \lim_{z\to \infty}\left[\frac{0.5\cdot\sigma'_{\text{V}}(z) + P_{\text{initial}}(z)}{\sigma'_{\text{V}}(z)}\right] \\ &= \lim_{z\to \infty}\left[\frac{\sigma_{\text{V}}(z)}{\sigma'_{\text{V}}(z)}\right] = \lim_{z\to \infty}\left[\frac{0.5\cdot\gamma_{\text{Rock}}\cdot z}{\left(\gamma_{\text{Rock}} - \gamma_{\text{Water}}\right)\cdot z}\right] \\ &= \frac{0.5\cdot 23}{23-10} = 0.9\end{aligned} \tag{17}$$

Interpretation of results based on Haimson and Fairhurst (1967).

For shallow depths, Haimson and Fairhurst's approach suggests that P_{HF} tends to the tensile strength of the rock, as shown in Eq. 18. The data in Fig. 6 confirm this theoretical observation, since the minimum $P_{\text{breakdown}}$ values are approximately 20 MPa for shallow hydraulic fracturing projects, larger than the vertical effective stresses at shallower depths, as explained in the next paragraph.

$$\lim_{z\to 0} P_{\text{HF}} = \lim_{z\to 0}\left[\sigma_{\text{t}} + 3S_{\text{h}}(z) - S_{\text{H}}(z) - P_{\text{initial}}(z)\right] = \sigma_{\text{t}} \tag{18}$$

Another important observation in Fig. 7 is that $\frac{P_{\text{breakdown}}}{\sigma'_{\text{V}}}$ tends to high values for shallower depths. Equation 19 shows that this result is expected if one interprets this observation using Haimson and Fairhurst.

$$\lim_{z\to 0} \frac{P_{\text{HF}}}{\sigma'_{\text{V}}} = \lim_{z\to 0}\left[\frac{\sigma_{\text{t}}}{\sigma'_{\text{V}}(z)}\right] = \infty \tag{19}$$

As vertical effective stresses increase (in other words, as z increases), Eq. 20 shows that P_{HF} tends to infinity. This corresponds to the trend shown in Fig. 6.

$$\lim_{z\to\infty} P_{HF} = \lim_{z\to\infty} \left[\sigma_t + 3S_h(z) - S_H(z) - P_{initial}(z)\right] = \infty \quad (20)$$

The data shown in Fig. 7 suggest that $\frac{P_{breakdown}}{\sigma'_V}$ tends to 1.0 for large depths. Two distinct in situ stress conditions were tested to conclude if there is a theoretical basis supporting this observation. For the condition $\sigma_V = S_H = S_h$, one obtains $\frac{P_{HF}}{\sigma'_V} \approx 2.7$ (Eq. 21), and for $S_H = 1.5 \cdot \sigma_V$ and $S_h = 0.75 \cdot \sigma_V$, one obtains $\frac{P_{HF}}{\sigma'_V} \approx 0.6 \ll 1.0$ (Eq. 22), which are not close to 1.0. This suggests that either (1) real projects may, in some cases, lead to $\frac{P_{breakdown}}{\sigma'_V} \ll 1.0$ for deep rocks; the limited number of deep projects investigated in this study (e.g., only four projects with $\sigma'_V > 50$MPa) may have introduced a bias in the observation that $\frac{P_{breakdown}}{\sigma'_V}$ tends to 1.0 for large depths, or (2) for deeper rocks, the very high in situ stresses lead to a breakdown dictated by the mobilization and extension of existing fractures (in other words, following the mechanism behind the Hubbert and Willis approach, which resulted in $\frac{P_{HF}}{\sigma'_V}$ closer to one), rather than through the initiation of new fractures, the mechanism in which Haimson and Fairhurst's approach is based on

$$\begin{aligned}\lim_{z\to\infty} \frac{P_{HF}}{\sigma'_V} &= \lim_{z\to\infty} \left[\frac{\sigma_t + 3\sigma_V(z) - \sigma_V(z) - P_{initial}(z)}{\sigma'_V(z)}\right] \\ &= \lim_{z\to\infty} \left[\frac{\sigma_t}{\sigma'_V(z)} + \frac{2\sigma_V(z) - P_{initial}(z)}{\sigma'_V(z)}\right] \\ &= 0 + \frac{2\cdot\gamma_{Rock} - \gamma_{Water}}{\gamma_{Rock} - \gamma_{Water}} = 2.8 \end{aligned} \quad (21)$$

$$\begin{aligned}\lim_{z\to\infty} \frac{P_{HF}}{\sigma'_V} &= \lim_{z\to\infty} \left[\frac{\sigma_t + 3\cdot 0.75\sigma_V(z) - 1.5\cdot\sigma_V(z) - P_{initial}(z)}{\sigma'_V(z)}\right] \\ &= \lim_{z\to\infty} \left[\frac{\sigma_t}{\sigma'_V(z)} + \frac{0.75\sigma_V(z) - P_{initial}(z)}{\sigma'_V(z)}\right] \\ &= 0 + \frac{0.75\cdot\gamma_{Rock} - \gamma_{Water}}{\gamma_{Rock} - \gamma_{Water}} = 0.6 \end{aligned} \quad (22)$$

5.2 Comparison with Theoretical Models

Based on the interpretation of the results, there appears to be three major reasons for the theoretical predictions to deviate from the measured breakdown pressures:

1. Mechanism of fracturing.

The approach proposed by Willis and Hubbert was derived to calculate the minimum pressure to "hold open and extend a fracture". Therefore, if the actual mechanism involved in one of the hydraulic fracturing projects investigated was the initial failure of the material and consequent initiation and propagation of the fracture, then the Willis and Hubbert approach may not yield the best estimate for the breakdown pressures, while Haimson and Fairhurst may be the most appropriate. The fact that Fig. 8 shows a good agreement between the shale projects (involve the initiation and subsequent propagation of new fractures) and Haimson and Fairhurst supports this assessment.

On the other hand, if the mechanism involved in the project was the mobilization and extension of an existing fracture then, by the earlier definition, Willis and Hubbert would be the most appropriate approach. The fact that the deeper projects in Fig. 8 show a good agreement with Willis and Hubbert also supports this interpretation.

It should also be noted that Haimson and Fairhurst is formulated based on the assumption that $\sigma_{\theta\theta}$ (refer to Fig. 3a) overcomes the tensile strength of the material. Geometrically, for this assumption to hold, a fracture parallel to the axis of the well (Fig. 3a) would have to occur. This fracture would develop when the minimum principal in situ stress is perpendicular to the axis of the well. From the cases analyzed in Table 3, this condition only applies to the Soultz, Fenton Hill, Basel projects, i.e., the minimum principal stress is S_h and the well is vertical. Based on the same physical reasoning, the other three projects (i.e., Bakken shale, Marcellus shale, Cooper Basin)—two of which are shale stimulations with horizontal wells—should have fractures developing perpendicularly to the axis of the well which is, in fact, common in oil/gas shale, i.e., the minimum principal stress is σ_V for the vertical well of Cooper Basin, and S_h for the shale projects, in which a horizontal well is typically drilled parallel to S_h. For this fracture geometry, however, one would theoretically require that σ_{zz}, rather than $\sigma_{\theta\theta}$ (refer to Fig. 3a), reaches the tensile strength of the material, since the fracture surfaces open in the zz direction as the fracture propagates in the rr direction (note that Haimson and Fairhurst is derived based on the assumption that $\sigma_{\theta\theta}$ reaches the tensile strength of the material). While thoroughly investigating how the assumed failure mechanisms affect the theoretical P_{HF} and P_{HW} would be a meaningful research exercise, this is, however, not in the scope of this technical note.

2. $P_{breakdown}$ is, by definition, larger than P_{HW} and P_{HF}.

As discussed in Sect. 2, the fracture initiation pressure, P_{HF} (FIP in Fig. 1), and the pressure necessary to "hold open and extend a fracture" (P_{HW}, or FPP in Fig. 1) are different from the formation breakdown pressure, $P_{breakdown}$ (FBP in Fig. 1). In fact, Fig. 1 shows that the formation breakdown pressure is typically higher than these theoretical pressures ($P_{breakdown} > P_{HW}$ and P_{HF}) which is, in general, supported by the data shown in Fig. 8.

3. Estimation of in situ stresses is based on assumptions.

It is complex to accurately measure the vertical and horizontal stresses in the field. In practice, empirical and theory-based estimates are often used to calculate the in situ stresses in hydraulic fracturing projects. Furthermore, in this study, the vertical stresses were estimated based on an average unit weight of the rock, which was the same for all the projects analyzed. The values are still reliable, since the unit weights of the analyzed rock formations do not vary significantly; however, it is recognized that this may be a source of errors and consequent deviations between the field observations and the theoretical models.

6 Summary and Conclusions

The breakdown pressures of several shale oil and/or gas and EGS hydraulic fracturing stimulations were related to the corresponding effective vertical stresses at the stimulated depths. Regardless of the type of the project, i.e., shale oil and/or gas or EGS, it was clear that $P_{breakdown}$ tends to a very small value for shallower formations and to infinity as the depth increases. It was also observed that the ratio between the breakdown pressures and effective vertical stresses, $\frac{P_{breakdown}}{\sigma'_v}$, is strongly affected by the effective vertical stresses at the bottom of the analyzed wells. For shallow stimulations, i.e., low effective stresses, the ratio $\frac{P_{breakdown}}{\sigma'_v}$ is usually larger than 2.0, while for deeper stimulations, i.e., high effective stresses, this ratio appears to approach 1.0.

These observations were evaluated and interpreted based on theoretical models. Both Hubbert and Willis (1957) and Haimson and Fairhurst (1967) models capture reasonably well the overall field observations, with Hubbert and Willis (1957), P_{HW}, accurately capturing the $P_{breakdown}$ measured in deeper projects, and Haimson and Fairhurst (1967), P_{HF} ,accurately predicting the $P_{breakdown}$ in shale projects. This was explained by the compatibility between the physical failure modes underlying the theoretical formulations of the two models and the likely fracturing mechanisms that occurred in the investigated field stimulations.

The results obtained in this study are important to better understand the phenomena involved in the hydraulic fracturing of rocks and, consequently, to more efficiently design hydraulic fracturing operations.

Acknowledgements The authors would like to express their gratitude for the support from NSF, through award number 1,738,081, under which the present study was conducted.

References

Agapito J, Hardy M (1982) Induced horizontal stress method of pillar design in oil shale. In: 15th oil shale symposium, Colorado School of Mines, pp. 191–197)

ASTM (2004) Standard test method for determination of the in-situ stress in rock using the hydraulic fracturing method. Annual Book of ASTM Standards D4645:1–8. https://doi.org/10.1520/D4645-08

Badra, H. (2011). Fracture characterization and analog modeling of the woodford shale in the arbuckle mountains, Oklahoma, USA. In: AAPG international conference and exhibition. Milan, Italy

Baisch S, Voros R (2009) AP 3000 report—induced seismicity. www.wsu.bs.ch. Accessed 10 Nov 2017

Bendall B, Hogarth R, Holl H, Mcmahon A, Larking A, Reid P (2014) Australian experiences in EGS permeability enhancement—a review of 3 case studies. In: Proceedings of 39th stanford geothermal workshop, pp 1–10

Berryman JG (2005) Poroelastic fluid effects on shear for rocks with soft anisotropy. Geophys J Int 161(3):881–890. https://doi.org/10.1111/j.1365-246X.2005.02581.x

Breit VS, Stright Jr DH, Dozzo JA (1992) Reservoir characterization of the bakken shale from modeling of horizontal well production interference data. In: SPE rocky mountain regional meeting. Casper, Wyoming: Society of Petroleum Engineers. https://doi.org/10.2118/24320-MS

Brown DW (2009) Hot dry rock geothermal energy: important lessons from Fenton Hill. In: Thirty-fourth workshop on geothermal reservoir engineering, 3–6

Brown DW, Duchane DV, Heiken G, Hriscu VT, Kron A (2012) Mining the earth's heat: hot dry rock geothermal energy. Mining the earth's heat: hot dry rock geothermal energy. Springer, New York. https://doi.org/10.1007/978-3-540-68910-2

Brudy M, Zoback MD, Fuchs K, Rummel F, Baumg'artner J (1997) Estimation of the complete stress tensor to 8 km depth in the KTB scientific drill holes' Implications for crustal strength. J Geophys Res 102(B8):18453–18475

Charles W, Bob B, Mike E, Tom L (2004) Improved horizontal well stimulations in the bakken formation, williston basin, montana. In: Proceedings of SPE annual technical conference and exhibition. https://doi.org/10.2523/90697-MS

Charléty J, Cuenot N, Dorbath L, Dorbath C, Haessler H, Frogneux M (2007) Large earthquakes during hydraulic stimulations at the geothermal site of Soultz-sous-Forêts. Int J Rock Mech Min Sci 44(8):1091–1105. https://doi.org/10.1016/j.ijrmms.2007.06.003

Cramer DD (1986) Reservoir characteristics and stimulation techniques in the bakken formation and adjacent beds, billings nose area, Williston Basin. Soc Petrol Eng. https://doi.org/10.2523/15166-MS

Detournay E, Cheng AHD (1993) Fundamentals of poroelasticity. In: Fairhurst C (ed) Comprehensive rock engineering: principles, practice and projects. Analysis and design methods, vol 2. Pergamon, Oxford/New York, pp 113–171

Dezayes C, Gentier S, Genter A (2005) Deep geothermal energy in Western Europe: the soultz project. BRGM/RP-54227-FR

Doherty P, Harrison R, Wallroth T (1994) Sensitivity study of the economics of heat pump basedhot dry rock (HDR) heating in Sweden. Report Fj-13

Eliasson T, Sundquist U, Wallroth T (1988) Rock mass characteristics at the HDR geothermal research site in the Bohus granite, SW Sweden

Engelder T, Lash GG, Uzcátegui RS (2009) Joint sets that enhance production from middle and upper devonian gas shales of the Appalachian Basin. AAPG Bull 93(7):857–889. https://doi.org/10.1306/03230908032

Fehler MC (1989) Stress control of seismicity patterns observed during hydraulic fracturing experiments at the Fenton Hill hot dry rock geothermal energy site, New Mexico. Int J Rock Mech Min Sci Geomech 26(3–4):211–219. https://doi.org/10.1016/0148-9062(89)91971-2

Feng Y, Gray KE (2017) Discussion on field injectivity tests during drilling. Rock Mech Rock Eng 50(2):493–498. https://doi.org/10.1007/s00603-016-1066-1

Fonseca ER, Farinas MJ (2013) Hydraulic fracturing simulation case study and post frac analysis in the haynesville shale. In: SPE hydraulic fracturing technology conference, (Xl). https://doi.org/10.2118/163847-MS

Fontaine J, Johnson N, Schoen D (2008) Design, execution, and evaluation of a "Typical" marcellus shale slickwater stimulation: a case history. Soc Petrol Eng. https://doi.org/10.2118/117772-MS

Frash L (2007) Laboratory-scale study of hydraulic fracturing in heterogeneous media for enhanced geothermal systems and general well stimulation (Ph.D Thesis). Civil and Environmental Engineering, Colorado School of Mines

Gale JFW, Reed RM, Holder J (2007) Natural fractures in the barnett shale and their importance for hydraulic fracture treatments. AAPG Bull 91(4):603–622. https://doi.org/10.1306/11010606061

Gray I (2017) Effective stress in rock. In: Wesseloo J, Wesseloo J (eds), eighth international conference on deep and high stress mining. perth: australian centre for geomechanics PP—Perth. https://papers.acg.uwa.edu.au/p/1704_12_Gray/

Grigsby CO, Tester JW (1989) Rock-water interactions in the Fenton Hill, New Mexico, hot dry rock geothermal systems. II. Modeling geochemical behavior. Geothermics 18(5–6):657–676. https://doi.org/10.1016/0375-6505(89)90099-0

Haimson B, Fairhurst C (1967) Initiation and extension of hydraulic fractures in rocks. Soc Petrol Eng 7(03):310–318. https://doi.org/10.2118/1710-PA

Haimson B, Zhao Z (1991) Effect of borehole size and pressurization rate on hydraulic fracturing breakdown pressure. In: The 32nd U.S. symposium on rock mechanics (USRMS), 10–12 July. American Rock Mechanics Association, pp 191–200

Häring MO, Schanz U, Ladner F, Dyer BC (2008) Characterisation of the Basel 1 enhanced geothermal system. Geothermics 37(5):469–495. https://doi.org/10.1016/j.geothermics.2008.06.002

Hill AJ, Gravestock DI (1995) Cooper basin. Geolo South Australia 2:78–87

Hirschmann G, Duyster J, Zulauf G, Kontny A, de Wall H, Lapp M, Harms U (2006) The KTB superdeep borehole: petrography and structure of a 9-km-deep crustal section. Geol Rundsch 86(S1):S3–S14. https://doi.org/10.1007/pl00014663

Hopkins CW, Holditch SA, Hill DG (1998) Characterization of an induced hydraulic fracture completion in a naturally fractured antrim shale reservoir, 177–185. https://doi.org/10.2118/51068-MS

Hubbert M, Willis D (1957) Mechanics of hydraulic fracturing. Soc Petrol Eng 9(6):153–166. https://doi.org/10.1016/S0376-7361(07)53011-6

O'Brien J, Duyster P, Grauert J, Schreyer W, Stockhert B, Weber K (1997) Crustal evolution of the KTB drill site: from oldest relies to the late Hercynian granites. J Geophys Res 102(B8):18203–18220

Jin Z, Li W, Jin C, Hambleton J, Cusatis G (2017) Elastic, strength, and fracture properties of marcellus shale. Int J Rock Mech Min Sci 109(17):124–137

Jost ML, Büßelberg T, Jost Ö, Harjes H-P (1998) Source parameters of injection-induced microearthquakes at 9 km depth at the KTB deep drilling site, Germany. Bull Seismol Soc Am 88(3):815–832

Jung R, Orzol J, Jatho R, Kehrer P, Tischner T (2005) The GeneSys-project: extraction of geothermal heat from tight sediments. In: Proceedings, 30th workshop on geothermal reservoir engineering, Stanford University, (April), 24–29

Jupe AJ, Green ASP, Wallroth T (1992) Induced microseismicity and reservoir growth at the Fjällbacka hot dry rocks project, Sweden. Int J Rock Mech Min Sci 29(4):343–354. https://doi.org/10.1016/0148-9062(92)90511-W

Kaieda H, Sasaki S, Wyborn D (2010) Comparison of characteristics of micro-earthquakes observed during hydraulic stimulation operations in Ogachi, Hijiori and Cooper Basin HDR projects. World Geothermal Congress 2010(April):1–6

Kitano K, Hori Y, Kaieda H (2000) Outline of the ogachi hdr project and character of the reservoirs. In: Proceedings of the world geothermal congress, Kyushu – Tohoku, Japan, pp 3773–3778

Konstantinos P (2005) Petrographic characterization of the Barnett Shale, Fort Worth Basin, Texas (MS.c Thesis). University of Texas at Austin, Austin, Texas

Kuhlman RD, Perez JI, Claiborne EB (1992) Microfracture stress tests, anelastic strain recovery, and differential strain analysis assist in bakken shale horizontal drilling program. SPE Rocky Mt Reg Meet. https://doi.org/10.2118/24379-MS

Laughlin AW, Eddy AC, Laney R, Aldrich MJ (1983) Geology of the Fenton Hill, New Mexico, hot dry rock site. J Volcanol Geotherm Res 15:21–41. https://doi.org/10.1016/0377-0273(83)90094-X

Matthew L, Ave B, Hall B, Timothy R (2009) Lithostratigraphy and petrophysics of the devonian marcellus interval in West Virginia and Southwestern Pennsylvania. In: 9th annual GCSSEPM foundation Bob F. perkins research conference. Houston, TX

Mayerhofer MJ, Stegent NA, Barth JO, Ryan KM (2011) Integrating fracture diagnostics and engineering data in the marcellus shale. In: SPE annual technical conference and exhibition, 30 October-2 November, Denver, Colorado, USA, 1–15. https://doi.org/10.2118/145463-MS

McClure, M. W. (2012). Modeling and characterization of hydraulic stimulation and induced seismicity in geothermal and shale gas reservoirs (Ph.D Thesis). Stanford University

McClure MW, Horne RN (2014) An investigation of stimulation mechanisms in enhanced geothermal systems. Int J Rock Mech Min Sci 72:242–260. https://doi.org/10.1016/j.ijrmms.2014.07.011

Montgomery SL, Jarvie DM, Bowker KA, Pollastro RM (2005) Mississippian Barnett Shale, Fort Worth basin, north-central Texas: gas-shale play with multi-trillion cubic foot potential. Am Asso Petrol Geol Bull 89(2):155–175. https://doi.org/10.1306/09170404042

Nunn J (2012) Burial and thermal history of the haynesville shale: implications for overpressure, gas generation, and natural hydrofracture. Gulf Coast Assoc Geol Soc 1(May):81–96

Phillips Z, Halverson R, Strauss S, Layman J, Green T (2007) A case study in the bakken formation: changes to hydraulic fracture stimulation treatments result in improved oil production and reduced treatment costs. In: Rocky mountain oil & gas technology symposium. Society of Petroleum Engineers. https://doi.org/10.2523/108045-MS

Richards JA, Walter LM, Budai JM, Abriola LM (1994) Large and small scale structural controls on fluid migration in the Antrim Shale, Northern Michigan basin. Advances in Antrim Shale Technology, Workshop, sponsored by Gas Research Institute in Cooperation with the Michigan Section Society of Petroleum Engineers, Mt. Pleasant, Michigan

Ryder RT (1990) Fracture patterns and their origin in the upper devonian antrim shale gas reservoir of the michigan basin: a review

Scott PP Jr, Bearden W, Howard GC (1953) Rock rupture as affected by fluid properties. J Petrol Technol 5:111–124. https://doi.org/10.2118/205-G

Shen B (2008) Borehole breakouts and in situ stresses. In: Potvin R, Carter Y, Dyskin J, Jeffrey A (ed) Proceedings of the first southern hemisphere international rock mechanics symposium, Australian Centre for Geomechanics, Perth, pp 407–418

Shin K, Ito H, Oikawa Y (2000) Stress stae at the Ogachi site. In: Proceedings world geothermal congress. Kyushu—Tohoku, Japan

Siebrits E, Elbel JL, Hoover RS, Diyashev IR, Griffin LG, Demetrius SL, Hill DG (2000) Refracture reorientation enhances gas production in barnett shale tight gas wells. Soc Petrol Eng. https://doi.org/10.2118/63030-MS

Tester JW (2006) The future of geothermal energy. Massachusetts Institute of Technology. http://www.eere.energy.gov/geothermal/pdfs/structure_outcome.pdf. Accessed 10 Oct 2017

Tischner T, Krug S, Hesshaus A, Jatho R, Bischoff M, Wonik T (2013) Massive fracturing in low permeable sedimentary rock in the GeneSys project. In: Proceedings of the thirty-eighth workshop on geothermal reservoir engineering geothermal reservoir engineering. Stanford University, Stanford, Califonia, USA

U.S. Energy Information Administration. (2011). Review of Emerging Resources: U.S. Shale Gas and Shale Oil Plays. https://www.eia.gov/analysis/studies/usshalegas/pdf/usshaleplays.pdf. Accessed 12 Oct 2017

Valley B, Evans KF (2007) Stress state at Soultz-Sous-Forets to 5 km depth from wellbore failure and hydraulic observations. In: Proceedings, thirty-second workshop on geothermal reservoir engineering stanford university, Stanford, California, SGP-TR-183

Vidal J, Genter A, Duringer P, Schmittbuhl J, Strasbourg U, De, Descartes R, Cedex F-S (2015) Natural permeability in fractured triassic sediments of the upper rhine graben from deep geothermal boreholes. In: World geothermal congress 2015 Melbourne, Australia, 19–25 April 2015, (April), 1–13

Wagner GA, Coyle DA, Duyster J, Peterek A, Schroder B, Wemmer K, Welzel B (1997) Post-variscan thermal and tectonic evolution of the KTB site and its surroundings. J Geophys Res 102(B8):18221–18232

Wallroth T (1990) Rock stress measurements at the HDR research site at Fjallbacka, Sweden. In: Baria R (ed) Camborne school of mines international hot dry rock conference. Robertson Scientific Publications, London, pp 98–107

Wallroth T, Eliasson T, Sundquist U (1999) Hot dry rock research experiments at Fjällbacka, Sweden. Geothermics 28(August):617–625. https://doi.org/10.1016/S0375-6505(99)00032-2

Wang C, Zeng Z (2011) Overview of Geomechanical Properties of Bakken Formation. In:Williston Basin, North Dakota. 45th U.S. Rock mechanics/geomechanics symposium. San Francisco, California: American Rock Mechanics Association

Wyborn D, De Graaf L, Davidson S, Hann S (2005) Development of Australia' s first hot fractured rock (HFR) underground heat exchanger, Cooper Basin, South Australia. Workshop Geothermal Congress 2005(April):24–29

Xin T (2014) Experimental and numerical study on evolution of biots coefficient during failure process for brittle rocks. Rock Mech Rock Eng 48:1289–1296

French S, Rodgerson J, Feik C (2014) Re-fracturing horizontal shale wells: case history of a woodford shale pilot project. Soc Petrol Eng. https://doi.org/10.2118/168607-MS

Yeager BB, Meyer BR (2010) Injection/fall-off testing in the marcellus shale: using reservoir knowledge to improve operational efficiency. SPE Eastern Regional Meeting, 13-15 October 2010, Morgantown, West Virginia, USA, (1975), 1–19. https://doi.org/10.2118/139067-MS

You M (2015) Strength criterion for rocks under compressive-tensile stresses and its application. J Rock Mech Geotech Eng 7(4):434–439. https://doi.org/10.1016/j.jrmge.2015.05.002

Zagorski WA, Wrightsone GR, Bowman DC (2012) The appalachian basin marcellus gas play: its history of development, geologic controls on production, and future potential as a world-class reservoir. Am Assoc Petrol Geologists Bull 97:98–107

Ziegler M, Valley B, Evans KF (2015) Characterisation of natural fractures an fracture zones of the basel EGS reservoir inferred from geophysical logging of the basel-1 well. In: World Geothermal Congress, April 19–25, Melbourne, Australia, (April), 19–25

Zoback MD, Moos D, Mastin L, Anderson RN (1985) Well Bore Breakouts and in-Situ Stress. J Geophys Res 90(B7):5523–5530. https://doi.org/10.1029/JB091iB14p14163